

## Interplay between Structure and Size in a Critical Crystal Nucleus

Daniele Moroni,<sup>1</sup> Pieter Rein ten Wolde,<sup>2</sup> and Peter G. Bolhuis<sup>1</sup>

<sup>1</sup>*van 't Hoff Institute for Molecular Sciences, Universiteit van Amsterdam, Nieuwe Achtergracht 166, 1018 WV Amsterdam, The Netherlands*

<sup>2</sup>*FOM Institute for Atomic and Molecular Physics, Kruislaan 407, 1098 SJ Amsterdam, The Netherlands*  
(Received 21 March 2005; published 16 June 2005)

We study the kinetics of crystal nucleation of an undercooled Lennard-Jones liquid using various path-sampling methods. We obtain the rate constant and elucidate the pathways for crystal nucleation. Analysis of the path ensemble reveals that crystal nucleation occurs along many different pathways, in which critical solid nuclei can be small, compact, and face centered cubic, but also large, less ordered, and more body centered cubic. The reaction coordinate thus includes, besides the cluster size, also the quality of the crystal structure.

DOI: 10.1103/PhysRevLett.94.235703

PACS numbers: 64.60.Qb, 07.05.Tp, 82.20.-w

An undercooled pure liquid is metastable with respect to the solid. Spontaneous crystallization can only occur via homogeneous nucleation, a thermally activated process involving the formation of a growing solid cluster. The qualitative understanding of crystal nucleation is based on the widely used classical nucleation theory (CNT), which gives a macroscopic description for the nucleation free-energy barrier and derives a transition state theory (TST) nucleation rate. However, the CNT predictions for the rate often differ orders of magnitude from the experimentally determined nucleation rates [1,2]. CNT assumes a spherical solid cluster consisting of the single most thermodynamically stable solid state, and neglects all kinetic effects. As a consequence, the only relevant parameter in CNT is the size of the solid cluster. Once nuclei have reached a critical size, they can grow to a bulk solid. In this Letter we show that not only the size, but also the shape, and more importantly, the structure, determine whether a nucleus is critical.

Computer simulations can give microscopic understanding, and, in particular, molecular dynamics (MD) appears to be a natural tool to study kinetics. However, even for a liquid as simple as Lennard-Jones (LJ), one has to go down to about 50% of the melting temperature to observe a single nucleation event in a simulation [3]. For lower undercooling both the critical nucleus and the barrier become larger and the CPU time to observe nucleation might exceed current computing power by orders of magnitude. To enable the computational study of the kinetics for such processes, the TST-based Bennett-Chandler method [4,5] writes the rate constant as a product of two factors: the equilibrium probability to be on the barrier and a kinetic prefactor. The first factor is given by the free-energy difference between the transition state region and the stable state. The second factor, the transmission coefficient, is obtained by firing off many trajectories from the top of the barrier.

The Bennett-Chandler approach is not only often used to determine the rate constant, but also to elucidate the mechanism of the transition. Ten Wolde *et al.* adopted

the procedure to study crystal nucleation in a LJ system at 20% undercooling [6–8]. Precritical nuclei were found to be mainly body centered cubic (bcc) ordered, in accordance with the scenario that the first nucleated phase for simple fluids is bcc [9]. As the nuclei grow to the critical size, the core develops a face centered cubic (fcc) phase. Critical and postcritical nuclei retain a diffuse bcc-like interface of approximately constant width.

For both the calculation of the free-energy barrier and the computation of the transmission coefficient, the Bennett-Chandler procedure requires an order parameter that serves as the reaction coordinate, i.e., measures the progress of the transition. The success of this approach depends strongly on the choice of the reaction coordinate. If poorly chosen, the system will sample the wrong part of the phase space, which will not only conceal the mechanism of the transition, but also hamper the evaluation of the transmission coefficient and thus the computation of the rate constant. For high dimensional complex systems a good reaction coordinate can be difficult to find and usually requires detailed *a priori* knowledge of the mechanism. In the case of nucleation, theoretical considerations suggest that fluctuations lead to deviations from CNT and that multiple cluster parameters are involved in the reaction coordinate [10].

The transition path-sampling (TPS) method [11,12] gathers a collection of trajectories connecting the reactant to the product stable region by employing a Monte Carlo (MC) algorithm. Because no *a priori* reaction coordinate is required, the resulting *path ensemble* gives an unbiased insight in the mechanism and kinetics of the reaction. Recently, TPS has been applied to study nucleation processes in an Ising model [13], boiling water [14], and a solid-solid transition [15].

The aim of this Letter is twofold. First, we show that using path sampling, it is possible to obtain the dynamics of crystal nucleation in a LJ fluid, without any biasing influence from the reaction coordinate choice, and to obtain accurate estimates for the rate constants and free-energy barriers. Second, and maybe most important, we

analyze the path ensemble using *committor* distributions [12]. We show that critical clusters can be small and compact, with a high degree of fcc ordering, but also loose and more bcc ordered.

Our system consists of  $N = 10648$  particles interacting through a standard truncated and shifted LJ potential. Throughout the Letter we use reduced units, such that the units of energy, length, mass, and time are unity. We simulated nucleation of the solid phase in the isobaric-isenthalpic  $NPH$  ensemble [16,17]. The pressure was fixed at  $P = 5.68$  [6] for which the theoretical melting temperature is  $T_m = 1.11$  [18]. The system was undercooled slowly at constant pressure from a fluid state at  $T = 2.0$  until  $T = 0.83$  and an enthalpy per particle  $H/N = 1.41$ . This corresponds to 25% degree of undercooling, which is comparable to Ref. [6].

We compute the nucleation rate constant  $k_{AB}$  by path sampling. At variance with TST, path sampling requires no single dividing surface separating the two stable states, but only a definition of both the reactant and product states in terms of an order parameter. We use  $n$ , the number of particles in the largest solid cluster in the system, and define the liquid state  $A$  by  $n < 26$  and the solid state  $B$  by  $n > 410$ . Configurations with  $n$  in between these values are neither liquid nor solid, but lie in the barrier region. To identify a particle as belonging to a solid cluster we characterize the local order around the particle by means of sixth order spherical harmonics [6]. Two solid particles belong to the same cluster if within a distance less than 1.5.

Because the TPS rate evaluation is computationally expensive, we employ the more efficient transition interface sampling (TIS) version of path sampling [19]. The partial path TIS (PPTIS) method [20] increases efficiency even more for diffusive processes by exploiting loss of correlation along trajectories and sampling much shorter paths. Both methods require a partition of phase space by  $l$  consecutive nonintersecting interfaces defined by  $n_i$ , with  $n_{i-1} < n_i$ , where  $n_0, n_l$  are the borders of state  $A$  and  $B$ , respectively. We stress that  $n$  must be able to distinguish the stable states, but is not required to correspond to the true reaction coordinate [19]. The rate constant can be written as  $k_{AB} = f_A * P(n_l|n_1)$ . The effective flux  $f_A$  out of  $A$  through interface  $n_1$  can be calculated by straightforward MD [19]. The second factor  $P(n|n_1)$ , the crossing probability of reaching interface  $n$  while coming directly from  $n_1$ , is iteratively computed along the interfaces in a series of path-sampling simulations [19]. TIS and PPTIS compute  $P(n|n_1)$  differently, but both employ the essential *shooting* and *path-reversal* MC moves to generate the paths [12]. Setting  $n_0 = 25.5$ ,  $n_1 = 30.5$ , and averaging over a series of 30 runs of time length 200, we obtained a flux  $f_A = 1.29 \pm 0.03$ . The TIS sampling was bootstrapped using a flux trajectory leaving  $A$  and crossing  $n_1$ . We performed a production run of 10 series of 100 paths each for the interfaces shown in Fig. 1. The re-

matched TIS crossing probability reaches a plateau value at  $n_l = 410.5$ , indicating commitment to complete solidification. The final crossing probability is  $P_A(n_l|n_1) = (8 \pm 6) \times 10^{-7}$ , and multiplying by the flux, the rate constant is  $k_{AB} = (1.0 \pm 0.8) \times 10^{-6}$ . The PPTIS simulations were also initiated using the trajectories from the flux calculation. The interfaces were chosen at  $n_i = 40.5 + 20 * (i - 2)$ , for  $i = 2, \dots, 38$ . A series of 100 simulations of 200 paths each was performed in a total of 37 windows. As seen in Fig. 1, the PPTIS crossing probability reaches a plateau at a value  $(1.4 \pm 0.9) \times 10^{-6}$ , which coincides with the plateau value of TIS within the error. Consequently, the final PPTIS rate constant  $k_{AB} = (2 \pm 1) \times 10^{-6}$  also coincides with the TIS rate. We thus conclude the system is diffusive enough to satisfy memory loss within our choice of interface separation.

By reweighting the paths properly [21], the free energy  $\beta G(n) = -\ln P(n)$  was computed during the PPTIS simulations (see inset Fig. 1). The barrier has a maximum at a cluster size  $n^* = 243$  for which  $\beta G(n^*) = 25.2 \pm 0.7$ . Using data from Ref. [6] the CNT free-energy barrier prediction for our conditions is  $\beta G^{\text{CNT}} = 5.3$ , a factor of 5 lower than our simulation results. The corresponding CNT nucleation rate  $k_{AB}^{\text{CNT}} = 4.6$  is 6 orders of magnitude higher than our simulation results. If we combine our simulation free-energy barrier with the CNT prefactor, the rate becomes  $k_{AB}^{\text{CNT}'} = 1.0 \times 10^{-8}$  which is now two orders too *low*. Similar results were found in Ref. [6]. These differences must be due to a failure of CNT to capture the molecular mechanism properly, which we will discuss below.

We investigated the crystallization mechanism in an ensemble of 84 uncorrelated paths generated at the last TIS interface, and extended until  $n > 1000$ , by considering many observables as possible reaction coordinates. Among others, we considered a set of bond-order parameters

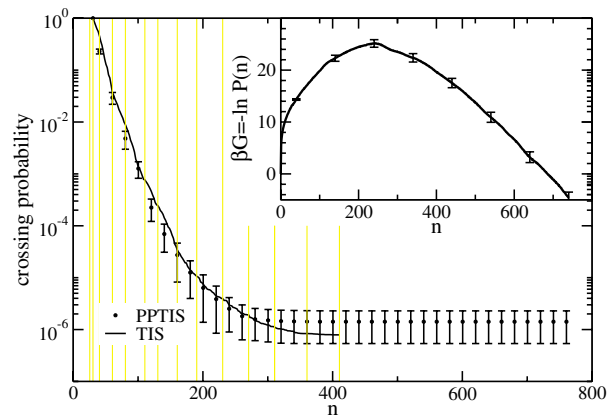


FIG. 1 (color online). TIS and PPTIS crossing probability. The position of TIS interfaces are given by vertical lines. The error on the TIS curve is comparable to the error of the PPTIS one. Inset: free energy  $-\ln P(n)$  from properly reweighted paths [21].

that are sensitive to the orientational ordering of the set of particles on which they are computed [6,22,23]. In particular, the cluster order parameter  $Q_6^{\text{cl}} = (\frac{4\pi}{13} \sum_{m=-6}^6 |\bar{Q}_{6m}|^2)^{1/2}$  gives an indication of the degree of the crystallinity within the solid cluster. It is constructed from the average  $\bar{Q}_{6m} = \frac{1}{N_b} \sum_{j=1}^{N_b} Y_{6m}(\hat{\mathbf{r}}_{ij})$ , where  $Y_{lm}(\hat{\mathbf{r}}_{ij})$  are spherical harmonics,  $\hat{\mathbf{r}}_{ij}$  a unit vector between  $i$  and its neighbor  $j$ , and the sum runs over the  $N_b$  bonds in the solid cluster. In addition, projecting the distribution of three different bond-order parameters onto predetermined distributions of equilibrated bcc, fcc, and liquid structures yields the fractions  $f_{\text{bcc}}$ ,  $f_{\text{fcc}}$ , and  $f_{\text{liq}}$ , respectively [6,24].

A typical transition path shows a gradual increase in  $n$ . The temperature increases slightly due to the latent heat release. Analysis of the gyration tensor [25] reveals that the cluster shape, averaged over trajectories, is chainlike for small cluster sizes, elongated at intermediate sizes, and only becomes spherical at large cluster size. During the nucleation the spherical stage is reached with quite a variance in the compactness of the cluster; some of the clusters grow compact, some retain a degree of elongation, indicating that nucleation takes place via multiple pathways. As  $n$  increases, the bcc fraction stays almost constant, while the liquid part decreases to make space for fcc particles. We can interpret this as a developing fcc core wetted by a bcc surface, but we do not see a sharp transition from a bcc- to a fcc-dominated structure at the top of the free-energy barrier (here  $n^* = 243$ ) [6].

For each saved configuration of each path in the path ensemble, we computed the *committer*  $p_B$  [12], the probability that a trajectory initiated from that configuration ends up in the solid state. A configuration with  $p_B = 0.5$  is denoted a critical nucleus, and the ensemble of such configurations is the transition state ensemble (TSE). Note that our definition of a critical cluster does *not* correspond to that of CNT, which assumes that a critical cluster is fully determined by its size. The committer of a typical trajec-

tory recrosses the  $p_B = 0.5$  surface several times before switching to the final solid state, and during the transition it visits again configurations committed to the liquid state at  $p_B = 0$ , showing the extremely diffusive behavior of the transition. Surprisingly, Fig. 2 shows that  $p_B(n)$  is not monotonic. States at  $p_B = 0$ , committed to the liquid phase, include configurations containing the smallest clusters, but also configurations with cluster sizes up to around 300. At the opposite side, states with  $p_B = 1$ , committed to the solid phase, do contain large clusters (up to above  $n = 1000$ ), but also clusters with sizes as small as 200. In the middle, configurations with increasing  $p_B$  have on average an increasing  $n$ , but with a large scatter of  $\pm 100$  in the data points. In particular, the cluster-size distribution of the TSE [26] at  $p_B = 0.5$  peaks around the free-energy maximum  $n^* = 243$ , but has a large width. Moreover, configurations having a cluster size  $n^* = 243$  actually exhibit an almost uniform committor distribution (see inset Fig. 2). For a proper reaction coordinate this distribution should be peaked around 0.5. Hence,  $n$  does not describe the process of nucleation completely and therefore is *not* a (sufficiently) good reaction coordinate.

Careful analysis led us to believe that  $Q_6^{\text{cl}}$  is an important component of the reaction coordinate for crystal nucleation. We therefore computed the two dimensional free energy  $\beta G(n, Q_6^{\text{cl}}) = -\ln P(n, Q_6^{\text{cl}})$  by umbrella sampling (Fig. 3). At first, the free-energy landscape seems to confirm the CNT description of crystal nucleation: the degree of crystallinity of the nuclei, as measured by  $Q_6^{\text{cl}}$ , remains fairly constant as the nuclei grow from a precritical size to their postcritical size. Indeed,  $n$  seems to be a good reaction coordinate as the lowest free-energy path from the liquid to the solid runs more or less parallel to the  $n$  axis.

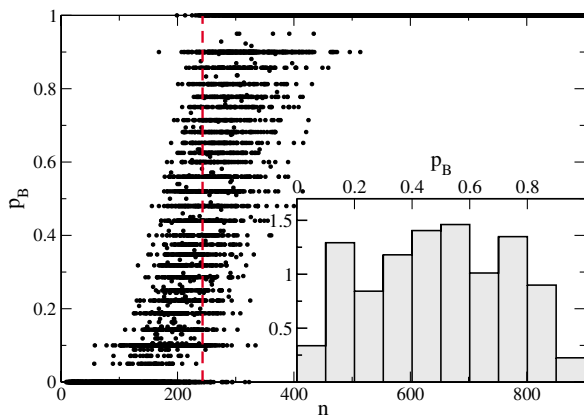


FIG. 2 (color online). Committer  $p_B$  as a function of  $n$  shows a large scattering. Inset: normalized committor distribution for  $n^* = 243$  (dashed line in main).

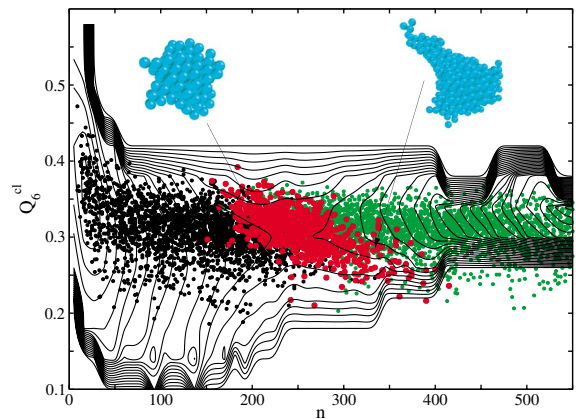


FIG. 3 (color). Contour plot of the free energy in the  $(n, Q_6^{\text{cl}})$  plane. The contour lines are separated by  $1k_B T$ . The transition state ensemble,  $p_B = 0.5$  (red circles), is shown, together with precritical ( $p_B = 0.1$ , black) and postcritical ( $p_B = 0.9$ , green) ensembles. At the top left we also show a compact dense fcc critical nucleus, corresponding to small  $n$  and large  $Q_6^{\text{cl}}$ , and to the right a cluster with a more mixed composition of fcc and bcc particles, corresponding to large  $n$  and small  $Q_6^{\text{cl}}$ .

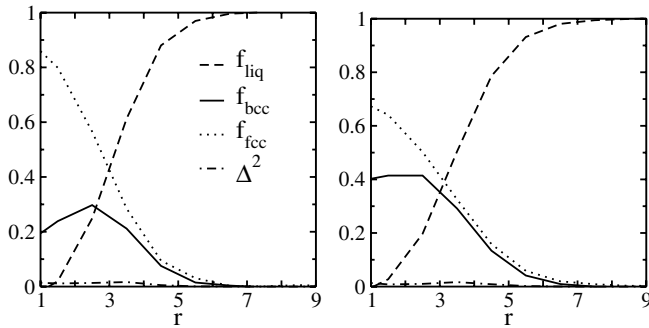


FIG. 4. Composition of the system around the center of mass of the critical clusters at  $p_B = 0.5$ . Small critical clusters ( $n < 230$ , left) are more fcc-like, while large critical clusters ( $n > 250$ , right) are more bcc-like.

However, plotting the TSE in the  $(n, Q_6^{\text{cl}})$  plane (see Fig. 3) reveals a clear correlation between  $Q_6^{\text{cl}}$  and  $n$ . In fact, the TSE is not perpendicular to the minimum free-energy path. Even though the transition states at  $p_B = 0.5$  are concentrated at the saddle point ( $n = 243$ ,  $Q_6^{\text{cl}} = 0.3$ ), the TSE exhibits configurations with large  $Q_6^{\text{cl}}$  and small  $n$  and vice versa. This clearly indicates that not only the size, but also the degree of crystallinity of the cluster, is an important order parameter for nucleation. This correlation is masked in the free-energy landscape.

Since most of the clusters in the TSE are roughly spherical, we can investigate their structural composition as a function of the distance  $r$  from the cluster center of mass for different subsets of the TSE (see Fig. 4). The bulk liquid structure is approached smoothly for large  $r$ , indicating that the surface is quite diffuse. More importantly, the crystalline structure of the critical clusters varies strongly, in contrast to the assumption of CNT that all critical nuclei consist of the thermodynamically most stable phase. In particular, we can distinguish the extremes of these critical clusters: (1) smaller compact clusters with a large fcc component in the core and a bcc component on the surface [Fig. 4(a)]; (2) larger clusters with a core less fcc and more bcc-like, indicating a looser, less well-packed cluster [Fig. 4(b)]. Analysis of postcritical clusters of the path ensemble revealed that these differences tend to disappear as all pathways converged to well structured fcc clusters. It is conceivable that at lower supercooling a single type of crystal structure dominates in the (larger) critical nuclei. We leave this for future work.

In summary, we find that homogeneous crystal nucleation proceeds via a range of pathways with fluctuations around the minimum free-energy path [10,13]. More surprisingly, the dynamical trajectories reveal a clear correlation in these fluctuations, which is concealed in the free-energy landscape. Whether a nucleus is critical is not only determined by its size, but also by its shape and structure. As this conclusion can probably be generalized to other

systems, an accurate theory of crystal nucleation must take into account the interplay between cluster size and cluster structure.

This work is part of the research program of the “Stichting voor Fundamenteel Onderzoek der Materie (FOM),” which is financially supported by the “Nederlandse organisatie voor Wetenschappelijk Onderzoek (NWO).”

- [1] D. Turnbull and J.C. Fischer, *J. Chem. Phys.* **17**, 71 (1949).
- [2] K. F. Kelton, in *Crystal Nucleation in Liquids and Glasses*, edited by H. Ehrenreich and D. Turnbull (Academic, New York, 1991), Vol. 45, pp. 75–177.
- [3] W. C. Swope and H. C. Andersen, *Phys. Rev. B* **41**, 7042 (1990).
- [4] C. H. Bennett, in *Algorithms for Chemical Computations*, edited by R. Christofferson, ACS Symposium Series No. 46 (American Chemical Society, Washington, D.C., 1977).
- [5] D. Chandler, *J. Chem. Phys.* **68**, 2959 (1978).
- [6] P. R. ten Wolde, M. J. Ruiz-Montero, and D. Frenkel, *Phys. Rev. Lett.* **75**, 2714 (1995).
- [7] P. R. ten Wolde, M. J. Ruiz-Montero, and D. Frenkel, *J. Chem. Phys.* **104**, 9932 (1996).
- [8] P. R. ten Wolde, M. J. Ruiz-Montero, and D. Frenkel, *Faraday Discuss.* **104**, 93 (1996).
- [9] S. Alexander and J. McTague, *Phys. Rev. Lett.* **41**, 702 (1978).
- [10] K. Binder and D. Stauffer, *Adv. Phys.* **25**, 343 (1976).
- [11] P. G. Bolhuis, D. Chandler, C. Dellago, and P. L. Geissler, *Annu. Rev. Phys. Chem.* **53**, 291 (2002).
- [12] C. Dellago, P. G. Bolhuis, and P. L. Geissler, *Adv. Chem. Phys.* **123**, 1 (2002).
- [13] A. C. Pan and D. Chandler, *J. Phys. Chem. B* **108**, 19681 (2004).
- [14] D. Zahn, *Phys. Rev. Lett.* **93**, 227801 (2004).
- [15] D. Zahn and S. Leoni, *Phys. Rev. Lett.* **92**, 250201 (2004).
- [16] H. C. Andersen, *J. Chem. Phys.* **72**, 2384 (1980).
- [17] G. J. Martyna, M. E. Tuckerman, D. J. Tobias, and M. L. Klein, *Mol. Phys.* **87**, 1117 (1996).
- [18] M. A. van der Hoef, *J. Chem. Phys.* **113**, 8142 (2000).
- [19] T. S. van Erp, D. Moroni, and P. G. Bolhuis, *J. Chem. Phys.* **118**, 7762 (2003).
- [20] D. Moroni, P. G. Bolhuis, and T. S. van Erp, *J. Chem. Phys.* **120**, 4055 (2004).
- [21] D. Moroni, T. S. van Erp, and P. G. Bolhuis, *Phys. Rev. E* **71**, 056709 (2005).
- [22] P. J. Steinhardt, D. R. Nelson, and M. Ronchetti, *Phys. Rev. B* **28**, 784 (1983).
- [23] J. S. van Duijneveldt and D. Frenkel, *J. Chem. Phys.* **96**, 4655 (1992).
- [24] The remainder  $\Delta^2$  is always small, showing that the projection decomposes the cluster structure quite well.
- [25] M. Fixman, *J. Chem. Phys.* **36**, 306 (1962).
- [26] The error in the computed committor is 0.1. So  $p_B = 0.5$  includes values in the range [0.4, 0.6].